energies

MDPI

Article

Organic Rankine Cycle Optimization Performance Analysis Based on Super-Heater Pressure: Comparison of Working Fluids

Ana Fernández-Guillamón [1,*,†], Ángel Molina-García [1,†], Francisco Vera-García [2,†] and José A. Almendros-Ibáñez [3,4,†]

1 Department of Automatics, Electrical Eng. and Electronic Tech., Universidad Politécnica de Cartagena, 30202 Cartagena, Spain; angel.molina@upct.es
2 Department of Thermal and Fluids Engineering, Universidad Politécnica de Cartagena, 30202 Cartagena, Spain; francisco.vera@upct.es
3 Department of Applied Mechanics and Project Engineering, Universidad de Castilla-La Mancha, 02001 Albacete, Spain; jose.almendros@uclm.es
4 Section of Energy Efficiency and Solar Energy, Renewable Energy Research Institute of Albacete, Universidad de Castilla-La Mancha, 02001 Albacete, Spain
* Correspondence: ana.fernandez@upct.es
† These authors contributed equally to this work.

Abstract: The organic Rankine cycle (ORC) is widely accepted to produce electricity from low-grade thermal heat sources. In fact, it is a developed technology for waste-heat to electricity conversions. In this paper, an ORC made up of super-heater, turbine, regenerator, condenser, pump, economizer and evaporator is considered. An optimization model to obtain the maximum performance of such ORC, depending on the super-heater pressure, is proposed and assessed, in order to find possible new working fluids that are less pollutant with similar behavior to those traditionally used. The different super-heater pressures under analysis lie in between the condenser pressure and 80% of the critical pressure of each working fluid, taking 100 values uniformly distributed. The system and optimization algorithm have been simulated in Matlab with the CoolProp library. Results show that the twelve working fluids can be categorized into four main groups, depending on the saturation pressure at ambient conditions (condenser pressure), observing that the fluids belonging to Group 1, which corresponds with the lower condensing pressure (around 100 kPa), provide the highest thermal efficiency, with values around $\eta = 23 - 25\%$. Moreover, it is also seen that R123 can be a good candidate to substitute R141B and R11; R114 can replace R236EA and R245FA; and both R1234ZE and R1234YF have similar behavior to R134A.

Keywords: organic Rankine cycle; maximum performance; optimum super-heater pressure; low-GWP; low-ODP; working fluids

Citation: Fernández-Guillamón, A.; Molina-García, Á.; Vera-García, F.; lmendros-Ibáñez, J.A. Organic Rankine Cycle Optimization Performance Analysis Based on Super-Heater Pressure: Comparison of Working Fluids. *Energies* **2021**, *14*, 2548. https://doi.org/10.3390/en14092548

Academic Editor: Francesco Calise

Received: 30 March 2021
Accepted: 27 April 2021
Published: 29 April 2021

1. Introduction

During the last decades, electricity demand has increased considerably, mainly due to population and industrial growth. The International Energy Agency estimates that the global electricity demand in 2030 will be 50% higher than in 2018 [1]. In fact, several scenarios until 2050 for both generation and demand trends have already been proposed and analyzed for different regions of the world [2–4]. Moreover, this electricity demand must be provided while reducing fossil fuel dependence, minimizing greenhouse emissions and promoting renewable energy sources (RESs) [5]. With this aim, different energy and climate policies have been promoted and supported to achieve such energy and climate targets [6], for instance, the U.S. Intended Nationally Determined Contribution [7], UK community energy strategy [8] and EU 2030 framework [9]. Under this scenario,

alternative technologies have emerged to convert renewable sources into electrical or/and mechanical energy.

With regard to electricity generation, thermal power plants are commonly included in current power systems. Steam power plants, which are most of the conventional power plants, are based on the Rankine cycle (RC) (i.e., coal-, nuclear- and oil-fueled power plants). Together with this, some RESs such as biomass-fueled, solar-thermal and geothermal power plants, use the RC to generate electricity. According to the International Energy Agency, which provides global statistics about electricity consumption [10], in 2018 more than 50% of the overall electricity generation came from power plants based on the RC, as can be seen in Table 1. For high-temperature applications and large power plants, water is considered the most suitable working fluid, whereas for medium- and small-scale power plants with low/intermediate temperature heat sources, the conventional steam RC cannot provide a high performance [11,12]. In such cases, organic Rankine cycle (ORC) systems, which use an appropriate organic working fluid instead of water, are considered as a mature and viable technology [13,14]. Moreover, the ORC has a high potential for waste heat recovery (WHR) applications, where the temperature level of waste heat is usually medium or low. For instance, waste energy in the exhaust gases of internal combustion engines (ICEs) can be exploited with WHR systems and the ORC, which are considered as the promising candidates for improving the global performance of ICEs. While industrial applications typically operate in steady conditions, there is a great challenge in coupling these two machines, the ICE and the ORC, due to the differences in their operating modes, transient in ICEs and stationary in the ORC. Consequently, the working fluid used in the ORC has a key role to determine the performance of the power plant [15–17] and to increase the performance for WHR systems, i.e., exhaust gases of ICEs [18,19].

Table 1. Generation by source in 2018 [10].

Source	Generation (GWh)	Rankine Cycle	Percentage (%)
Coal	10,159,646	Yes	38.01
Natural gas	6,150,200	No	–
Hydro-power	4,325,111	No	–
Nuclear	2,710,430	Yes	10.14
Wind	1,273,409	No	–
Oil	783,703	Yes	2.93
Biomass	637,240	Yes	2.38
PV	554,382	No	–
Geothermal	88,956	Yes	0.33
Others	35,669	No	–
Solar thermal	11,321	Yes	0.04
Total	26,730,067	–	53.84

Regarding the organic working fluids, two main parameters must be taken into account from the environmental point of view: (i) the ozone-depleting potential (ODP), which shows the impact of the fluid on the ozone depletion; and (ii) the global warming potential (GWP), which determines the greenhouse effect of the fluid [20]. In 2006, Europe started to limit the emissions from air conditioning systems in motor vehicles with Directive 2006/40/EC [21]. These limitations continued in 2014 with Regulation No 517/2014 on fluorinated greenhouse gases [22]. Restrictions to working fluids with high GWP and ODP have been approved in most developed countries around the world [23] and, consequently, new working fluids with less environmental impact have been under development, such as R1234YF and R1234ZE [24]. In fact, some working fluids can increase the greenhouse gas emissions, which, at the same time, cause ozone depletion [25]. Consequently, the fluids with low GWP and ODP must substitute those with higher GWP and ODP and, at the same time, try to maintain—or even increase—the overall efficiency of the ORC [26]. Hence,

optimization of the main ORC components and working fluids are currently major research fields to improve the ORC system performance [27].

In the specific literature, there are a few studies focused on comparing different low GWP and/or ODP working fluids among multiple alternatives. For instance, in [28] three low-GWP fluids were investigated in an ORC system to replace R245FA; Gil et al. identified different hydrofluoroolefins and their application in the ejector refrigeration cycle to substitute fluid R134A [29]; and in [30], an analysis about the working fluid R463A as an alternative to R404A was carried out. Under this scenario, this paper aims to optimize an ORC system using a variety of new working fluids with low GWP and ODP (R114, R123, R1234YF and R1234ZE), comparing them to conventional fluids (R11, R134A, R141B, R236EAL R244FA and R507A, as well as ammonia and water). The proposed methodology uses an iterative analysis to optimize the ORC system performance in the steady-state, based on the critical temperature of the fluid and depending on the super-heater pressure. Different working fluid groups are proposed depending on such output super-heater range pressures and maximum efficiency, specifying in each case which working fluid is preferable to use based on GWP and ODP.

The rest of the paper is structured as follows: Section 2 describes the ORC under analysis considering a steady-state and two cycles, excluding and including irreversibilities; Section 3 presents the proposed methodology; Section 4 analyzes and discusses the results; and, finally, conclusions are given in Section 5.

2. Organic Rankine Thermodynamic Cycle Under Analysis

The ORC under analysis consists of seven main elements: (i) super-heater, (ii) turbine, (iii) regenerator, (iv) condenser, (v) pump, (vi) economizer and (vii) evaporator. Both the elements and the T–s diagram are depicted in Figure 1. Two cycles are considered in the analysis: the ideal cycle (in which irreversibilities are not considered) and a second cycle including the irreversibilities in the turbine (η_t) and in the pump (η_p). The ideal cycle is represented in the T–s diagram with the states $1s$ and $6s$ (for the pump and turbine, respectively), whereas when considering the irreversibilities, such states are denoted as 1 and 6. Referring to such figure, note that the working fluid follows several processes:

- Process 1–2: The working fluid increases its temperature as it flows at constant pressure through the regenerator;
- Process 2–3: The working fluid increases its temperature until it is a saturated liquid as it flows at constant pressure through the economizer;
- Process 3–4: The working fluid keeps its temperature and pressure while changing from saturated liquid to saturated steam through the evaporator;
- Process 4–5: The working fluid increases its temperature as it flows at constant pressure through the super-heater;
- Process 5–6: The working fluid expands through the turbine, reducing both temperature and pressure;
- Process 6–8: The working fluid decreases its temperature as it flows at constant pressure through the regenerator;
- Process 8–9: The working fluid transfers heat as it flows through the condenser to the saturated liquid;
- Process 9–1: The working fluid compresses in the pump, increasing both temperature and pressure to the liquid region.

Note that the turbine shaft is directly connected to an electrical generator (point 7, saturated steam).

From Figure 1b, it is deduced that

$$p_1 = p_2 = p_3 = p_4 = p_5\,, \tag{1}$$

and

$$p_6 = p_7 = p_8 = p_9\,. \tag{2}$$

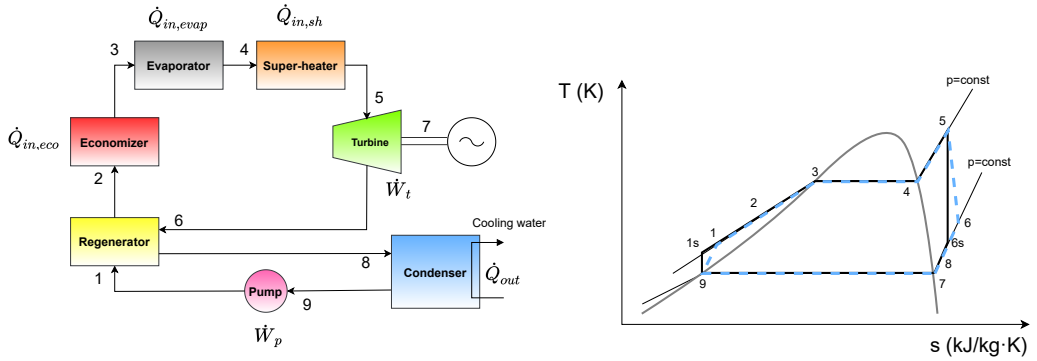

(**a**) (**b**)

Figure 1. ORC cycle under analysis. (**a**) Elements; (**b**) T–s diagram.

To determine the rest of the parameters (temperature T, quality x, enthalpy h and entropy s):

- Note that some states are saturated (liquid or vapor). In fact, states 4 and 7 are saturated vapor ($x_4 = x_7 = 1$), whereas 3 and 9 are saturated liquid ($x_3 = x_9 = 0$), as previously presented.
- To calculate the temperatures of the different states, all of them are determined from other parameters, but for state 2, where it considers the effectiveness of the regenerator (ε_{reg}):

$$T_2 = T_1 + \varepsilon_{reg} \cdot (T_6 - T_1)\,. \tag{3}$$

  It is important to bear in mind that T_2 must be in the liquid state, not being allowed a phase change. Temperature for state 5 (T_5) is assumed to be known, and it is equal to the critical temperature (T_{crit}) of the working fluid according to [31]. These authors found out that the global exergy efficiency is strongly linked to the critical temperature of the working fluid. The temperature of the regenerator (T_8) is considered as 2 °C over the saturated temperature at p_8.
- Most of the enthalpies are obtained knowing the temperature and pressure of each state. Only for states 1 (h_1) and 6 (h_6) are the energy balance of the pump (Equation (4)) and the turbine efficiency (η_t, Equation (5)) needed, respectively:

$$h_1 = h_9 + W_p\,, \tag{4}$$

$$h_6 = h_5 - \eta_t \cdot (h_5 - h_{6s})\,. \tag{5}$$

- The entropies are obtained knowing the pressure and enthalpy of each state.

With the different enthalpies calculated, it is possible to determine the specific work developed by the turbine (W_t):

$$W_t = h_5 - h_6\,, \tag{6}$$

as well as the specific thermal power exchanged in the economizer ($Q_{in,eco}$), evaporator ($Q_{in,evap}$) and super-heater ($Q_{in,sh}$):

$$Q_{in,eco} = h_3 - h_2\,, \tag{7}$$

$$Q_{in,evap} = h_4 - h_3\,, \tag{8}$$

$$Q_{in,sh} = h_5 - h_4\,. \tag{9}$$

The specific work demanded by the pump is calculated with the isoentropic value. The pump efficiency is then determined as:

$$W_{p,s} = v9 \cdot (p1 - p9) \rightarrow W_p = \frac{W_{p,s}}{\eta_p}. \tag{10}$$

The overall performance of the ORC is estimated from:

$$\eta(\%) = 100 \cdot \frac{W_{net}}{Q_{in}}, \tag{11}$$

where W_{net} is the net specific work developed by the cycle and Q_{in} is the specific thermal power supplied to the cycle:

$$W_{net} = W_t - W_p, \tag{12}$$

$$Q_{in} = Q_{in,eco} + Q_{in,evap} + Q_{in,sh}. \tag{13}$$

3. Methodology

The aim of the paper is to determine the maximum performance of the ORC presented in Section 2 as a function of the super-heater pressure. In order to determine such parameter, several aspects are taken into account:

- The pressure of the condenser ($p_{cond} = p_6 = p_7 = p_8 = p_9$) is determined considering a 293.15 K temperature and a saturated state [32,33] $\rightarrow p_{cond} = p(x = 1, T = 293.15\,\text{K})$;
- The pressure of the super-heater ($p_{sh} = p_1 = p_2 = p_3 = p_4 = p_5$) stays in between the pressure of the condenser and 80% of the critical pressure p_{crit} of the working fluid [34]. A homogeneous distribution of 100 values of p_{sh} are considered to determine the optimum value for maximum performance $\rightarrow p_{sh,min} = p_{cond}$; $p_{sh,max} = 0.8 \cdot p_{crit}$;
- When considering the irreversibilities of the turbine and the pump, their performances are 85% [35] and 80% [36,37], respectively $\rightarrow \eta_t = 0.85$; $\eta_p = 0.80$;
- The effectiveness of the regenerator is considered as 50%. According to the literature review, several values are proposed [38–41], and authors decide to use an averaged value $\rightarrow \varepsilon_{reg} = 0.5$;
- The output temperature of the super-heater (T_5) is considered to be equal to the critical temperature T_{crit} of the working fluid, as explained in Section 2 $\rightarrow T_5 = T_{crit}$;
- In case the state 6 is inside the saturation curve, its quality must be over 90% [42] $\rightarrow x_6 > 0.9$.

Twelve different working-fluids were selected for analysis, summarized in Table 2. Their critical pressure (p_{crit}), the maximum super-heater pressure ($p_{sh,max}$), the critical temperature (T_{crit}), which will be equal to the output temperature of the super-heater (T_5), GWP and ODP are included in the table. Among them, R134A and R141B are common working fluids [43], together with water, which is the fluid used to carry out the conventional RC [44]. Moreover, R134A and 1234YF have previously been analyzed by some of the authors of this work [45,46]. Together with this, R114, R123, R1234YF and R1234ZE have both low ODP and GWP (GWP < 150), and the authors' aim is to try to replace conventional pollutant working fluids with less-contaminant fluids, at the time that the overall efficiency of the ORC is improved.

Table 2. Working fluids under analysis [47–54].

Name	p_{crit} (kPa)	$p_{sh,max}$ (kPa)	T_{crit} (K)	GWP (100 Years)	ODP
R11	4394.00	3515.20	471.06	4000	1
R114	3257.00	2605.60	418.83	3.9	0
R123	3672.00	2937.60	456.83	77	0.02
R1234YF	3382.20	2705.76	367.85	4	0
R1234ZE	3634.94	2907.95	382.52	6	0
R134A	4059.28	3247.42	374.21	1300	0
R141B	4212.00	3369.60	477.50	630	0.11
R236EA	3420.00	2736.00	412.44	710	0

Table 2. *Cont.*

Name	p_{crit} (kPa)	$p_{sh,max}$ (kPa)	T_{crit} (K)	GWP (100 Years)	ODP
R245FA	3651.00	2920.80	427.01	950	0
R507A	3704.90	2963.92	343.77	3300	0
Ammonia	11,333.00	9066.40	405.40	0	0
Water	22,064.00	17,651.20	647.10	0	0

The Matlab commercial software package, combined with the CoolProp library [47] was used to optimize the cycle performance through an iterative process. The maximum performance (η_{max}) and optimum super-heater pressure ($p_{sh,opt}$) for the ORC presented in Section 2 are determined as follows, see Figure 2.

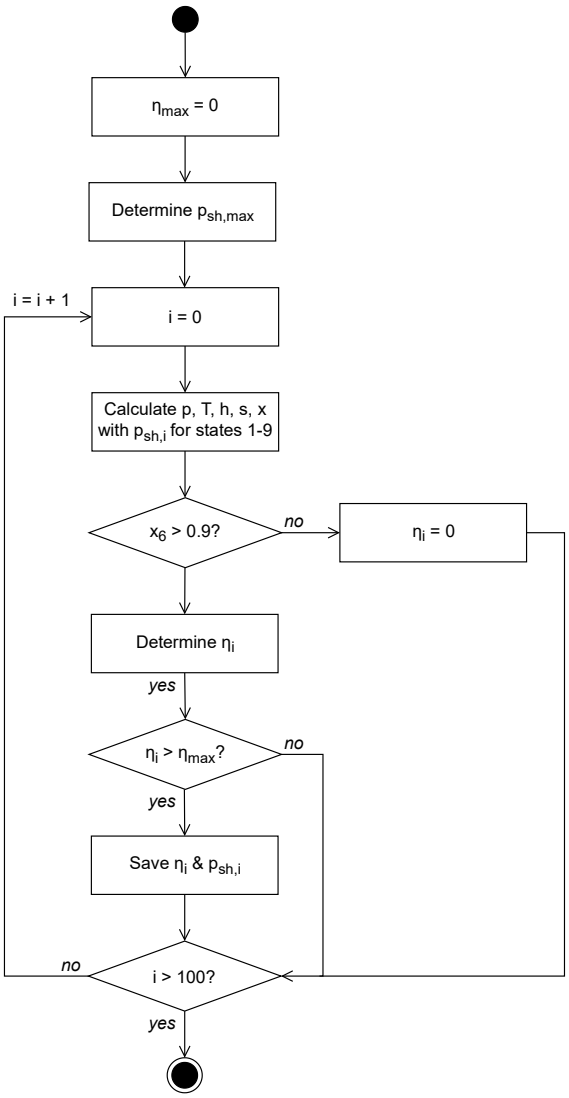

Figure 2. Flowchart to determine the maximum performance and the super-heater pressure.

1. To determine the maximum performance of the fluid, the initial performance is set as $\eta_{max,[i=0]} = 0\%$. The performance is compared to the previous maximum performance for each iteration, and it is increased depending on such comparison.
2. The maximum super-heater pressure ($p_{sh,max}$) is estimated from $p_{sh,max} = 0.8 \cdot p_{crit}$ (refer to Table 2). The minimum super-heater pressure will be equal to the condenser pressure $p_{sh,min} = p_{cond}$, which is calculated from the temperature of 293.15 K and knowing it is in saturated state. From such two pressures ($p_{sh,min}$ and $p_{sh,max}$),

100 values of pressure are uniformly distributed. These 100 values are the super-heater pressures ($p_{sh,i}$) that will be tested to determine the maximum cycle performance.

3. The different variables of the 9 states of the ORC depicted in Figure 1 are determined (p, T, h, s and x).
4. They are tested if the quality of state 6 (x_6) is over 90%:
   (a) If the quality is over 90% ($x_6 > 0.9$), the algorithm proceeds to the next step.
   (b) If the quality is below 90% ($x_6 \leq 0.9$), the cycle cannot take place due to the erosion of the turbine blades [42]. Consequently, the cycle performance is set to 0 ($\eta_i = 0$) and the algorithm goes to the last step.
5. The performance of the cycle (η_i) is calculated from Equation (11) and it is compared with the maximum performance:
   (a) If the performance of the cycle exceeds the maximum performance ($\eta_i > \eta_{max}$), the value of η_{max} is updated ($\eta_{max} = \eta_i$) and the super-heater pressure ($p_{sh,i}$) is saved. After that, the algorithm proceeds.
   (b) If the performance of the cycle does not exceed the maximum performance ($\eta_i < \eta_{max}$), the algorithm goes to the last step.
6. The following ($i = i + 1$) super-heater pressure is determined, repeating the algorithm from step 3. It finishes when the 100 values of $p_{sh,i}$ have been considered to determine the optimum performance ($i > 100$).

4. Results

The algorithm presented in Section 3 was run for the 12 working fluids under analysis (refer to Table 2) in Matlab and the CoolProp library. The maximum performance of the ORC (η_{max}), together with the optimum super-heater pressure ($p_{sh,opt}$) were obtained. These results are summarized in Table 3. As can be seen, when considering the irreversibilities of the turbine and the pump, the maximum performance is slightly reduced, as the performances of such elements are considered ($\eta_t = 0.85; \eta_p = 0.80$). It is also interesting to remark that the optimum super-heater pressure ($p_{sh,opt}$) is not always the same for both ideal and real cycles (R11, R123, R134A, R141B, R245FA, ammonia and water). However, in such cases, both optimum super-heater pressures are similar, with a maximum difference of 2.5% for the working fluid R245FA. Only for ammonia and water is such difference increased, as the quality at the turbine output is not fulfilled in many cases. For the other five fluids (R11, R141, R1234YF, R1234ZE and R236EA), this optimum pressure ($p_{sh,opt}$) is the same for both cycles, and equal to the maximum value considered ($p_{sh,max}$), which was set to 80% of the critical pressure, as presented in Section 3. Figure 3 shows two examples of working fluids, including both the ideal and real ORC, and the maximum performances (η_{max}) and the super-heater pressures at which such η_{max} are obtained. As can be seen, working fluid R141B reaches its maximum performance at different super-heater pressures depending on the kind of ORC (ideal or real), as was mentioned previously. In contrast, R1234YF achieves the maximum performance at the same super-heater pressure, which matches up with the last pressure considered. The reason why some working fluids get their performance at such maximum super-heater pressure under analysis is due to Carnot's efficiency, as the higher the heat input temperature of the hot source, the higher the equivalent cycle efficiency.

Table 3. Maximum performance (η_{max}), optimum super-heater pressure ($p_{sh,opt}$) and output super-heater temperature (T_5) for each working fluid under analysis.

		Ideal Cycle	Real Cycle
R11	η_{max} (%)	27.3	23.7
	$p_{sh,opt}$ (kPa)	3099.9	3030.6
	T_5 (K)	471.1	471.1

Table 3. *Cont.*

		Ideal Cycle	Real Cycle
R114	η_{max} (%)	21.8	18.6
	$p_{sh,opt}$ (kPa)	2605.6	2605.6
	T_5 (K)	418.8	418.8
R123	η_{max} (%)	26.2	22.7
	$p_{sh,opt}$ (kPa)	2793.1	2764.1
	T_5 (K)	456.8	456.8
R1234YF	η_{max} (%)	14.6	12.2
	$p_{sh,opt}$ (kPa)	2705.8	2705.8
	T_5 (K)	367.9	367.9
R1234ZE	η_{max} (%)	16.8	14.2
	$p_{sh,opt}$ (kPa)	2907.9	2907.9
	T_5 (K)	382.5	382.5
R134A	η_{max} (%)	15.4	12.9
	$p_{sh,opt}$ (kPa)	3247.4	3166.3
	T_5 (K)	374.2	374.2
R141B	η_{max} (%)	28.4	24.6
	$p_{sh,opt}$ (kPa)	3102.6	3069.2
	T_5 (K)	477.5	477.5
R236EA	η_{max} (%)	21.1	18.0
	$p_{sh,opt}$ (kPa)	2736.0	2736.0
	T_5 (K)	412.4	412.4
R245FA	η_{max} (%)	22.9	19.7
	$p_{sh,opt}$ (kPa)	2892.5	2836.0
	T_5 (K)	427.0	427.0
R507A	η_{max} (%)	10.3	8.4
	$p_{sh,opt}$ (kPa)	2963.9	2963.9
	T_5 (K)	343.8	343.8
Ammonia	η_{max} (%)	18.60	16.23
	$p_{sh,opt}$ (kPa)	5998.3	6910.4
	T_5 (K)	405.4	405.4
Water	η_{max} (%)	29.22	28.71
	$p_{sh,opt}$ (kPa)	358.88	1072
	T_5 (K)	647.1	647.1

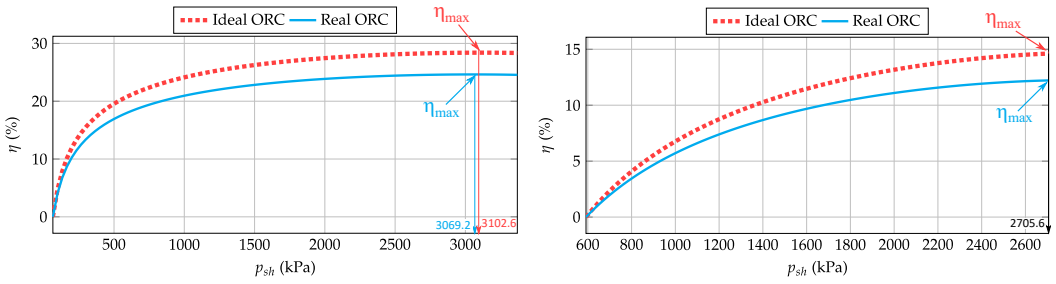

(**a**) (**b**)

Figure 3. Example of performance evolution for two working fluids considering ideal and real ORC. (**a**) R141B; (**b**) R1234YF.

In Figure 4, the evolution of the real ORC performance for most of the fluids is depicted. Only ammonia and water are excluded, and will later be analyzed in Figure 5. From Figure 4, four different groups of working fluids can be identified:

- Group 1. These fluids start to carry out the ORC even if the super-heater pressure is $p_{sh} \approx 100$ kPa. They quickly increase the performance of the ORC. In fact, they have performances around 20% for $p_{sh} \approx 1000$ kPa. The maximum performances are in between 23 and 25% for $3000 \leq p_{sh} \leq 3600$ kPa. R141B, R11 and R123 are included in this group. Moreover, the output temperature of the super-heater (T_5) for these working fluids is in the range $450 \leq T_5 \leq 480$ K. Among the three working fluids included in Group 1, the authors recommend the use of R123 due to the lower values of GWP and ODP.
- Group 2. These working fluids start to carry out the ORC for super-heater pressures between $100 \leq p_{sh} \leq 200$ kPa. Their performances do not increase as quickly as for Group 1, having performances around 15% for $p_{sh} \approx 1000$ kPa. The maximum performances are in between 15 and 20% for $2500 \leq p_{sh} \leq 3000$ kPa. This group includes R245FA, R114 and R236EA, which have an output temperature of the super-heater (T_5) in between $410 \leq T_5 \leq 430$ K. Among the three working fluids included in Group 2, the authors recommend the use of R114 due to the lower values of GWP and ODP.
- Group 3. They need a super-heater pressure between $400 \leq p_{sh} \leq 600$ kPa to start to carry out the thermodynamic cycle. The performance increases slower than in the two previous groups, with values between 5 and 10% for $p_{sh} \approx 1000$ kPa. Moreover, their maximum performances are in between 10 and 15% for $2500 \leq p_{sh} \leq 3000$ kPa. R1234ZE, R134A and R1234YF are included in this group. In this case, the output temperature of the super-heater (T_5) is in the range $360 \leq T_5 \leq 380$ K. Among the three working fluids included in Group 3, the authors recommend the use of R1234ZE and/or R1234YF due to the lower values of GWP and ODP. This has previously been proposed in several works [55–57].
- Group 4. They need a super-heater pressure over $p_{sh} \geq 1000$ kPa to start to carry out the thermodynamic cycle. The performance increases very slowly, with a maximum value under 10% for $p_{sh} \approx 3000$ kPa. This group includes R507A, which has an output super-heater temperature of $T_5 \leq 350$ K.

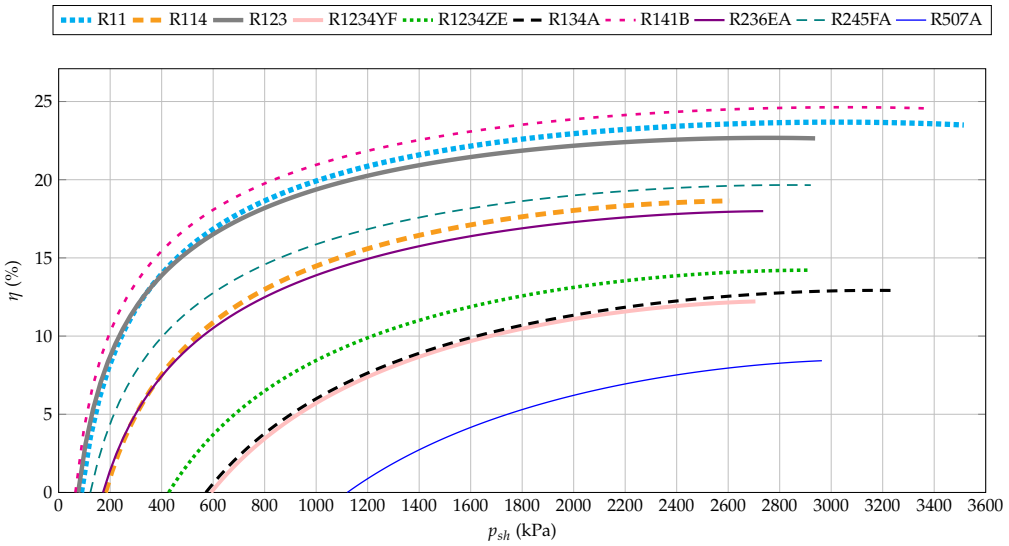

Figure 4. Performance evolution considering real ORC.

As a consequence, those working fluids included in Group 1 are the best option for ORC installations, as they have the widest super-heater pressure range together with the highest overall performance.

Figure 5 depicts the performance evolution considering water and ammonia as working fluids. In these cases, the quality of the fluids in state 6 is inside the saturation curve. Consequently, there are several super-heater pressures that cannot be used, as the quality of the fluid at the output of the turbine is under 90%. Ammonia can only work between $4000 \leq p_{sh} \leq 7000$ kPa, with a maximum performance between 10 and 20%. In contrast, the ORC with water as the working fluid can have a performance up to 30%. Indeed, a performance in between $20 \leq \eta \leq 30\%$ is reached with a super-heater pressure in the range $180 \leq p_{sh} \leq 1000$ kPa. Consequently, it can be considered as a working fluid of Group 1, following the categorization previously proposed and analyzed. The main difference between water and the working fluids included in Group 1 is the output temperature of the super-heater (T_5), which is 650 K for water, around 200 K over the range of the working fluids included in Group 1 ($450 \leq T_5 \leq 480$ K).

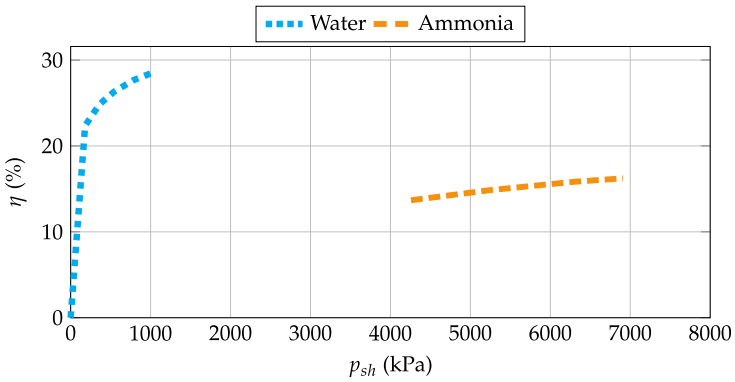

Figure 5. Performance evolution for water and ammonia considering real ORC.

Figures 6–8 show the T–s diagrams for working fluid Groups 1 and 2, Groups 3 and 4, and ammonia and water, respectively. Only the real ORCs are presented for the sake of clarity. Note that the same X (0 kJ/(kg K) $\leq X \leq$ 9 kJ/(kg K)) and Y (200 K $\leq Y \leq$ 700 K) axis limits are considered in the three figures, in order to ease the comprehension of the diagrams. With these figures, it is easy to understand the four groups previously defined, as they have similar T–s diagrams and similar differences between the super-heater pressure and the condenser pressure, which, in fact, causes the similar behavior of the performance of the ORC with fluids of the same group, as shown in Figure 4. In addition, an important difference between the T–s diagram of the organic fluids and those of water and ammonia can be seen, not only because of the higher temperatures and entropies of water and ammonia, but also because of the symmetry of the saturation curve in these two fluids. Together with this, Figure 8 also depicts the fact that state 6 for both ammonia and water lies inside the saturation curve, whereas it is outside for the other organic working fluids (refer to Figures 6 and 7).

In Figure 9 the maximum performance of the ORC depending on the fluid and the output super-heater temperature is presented. Organic fluids are grouped according to the classification proposed from Figure 4. Considering this figure, ammonia could be included in Group 2, as the output super-heater temperature is within the range specified for such group ($410 \leq T_5 \leq 430$ K) and similar maximum performance of the ORC ($\eta_{max} \approx 16\%$) is obtained. However, its super-heater pressure to reach that maximum performance is nearly 7000 kPa, which is twice the value of the super-heater pressure needed in the organic fluids of Group 2 to obtain a similar maximum performance.

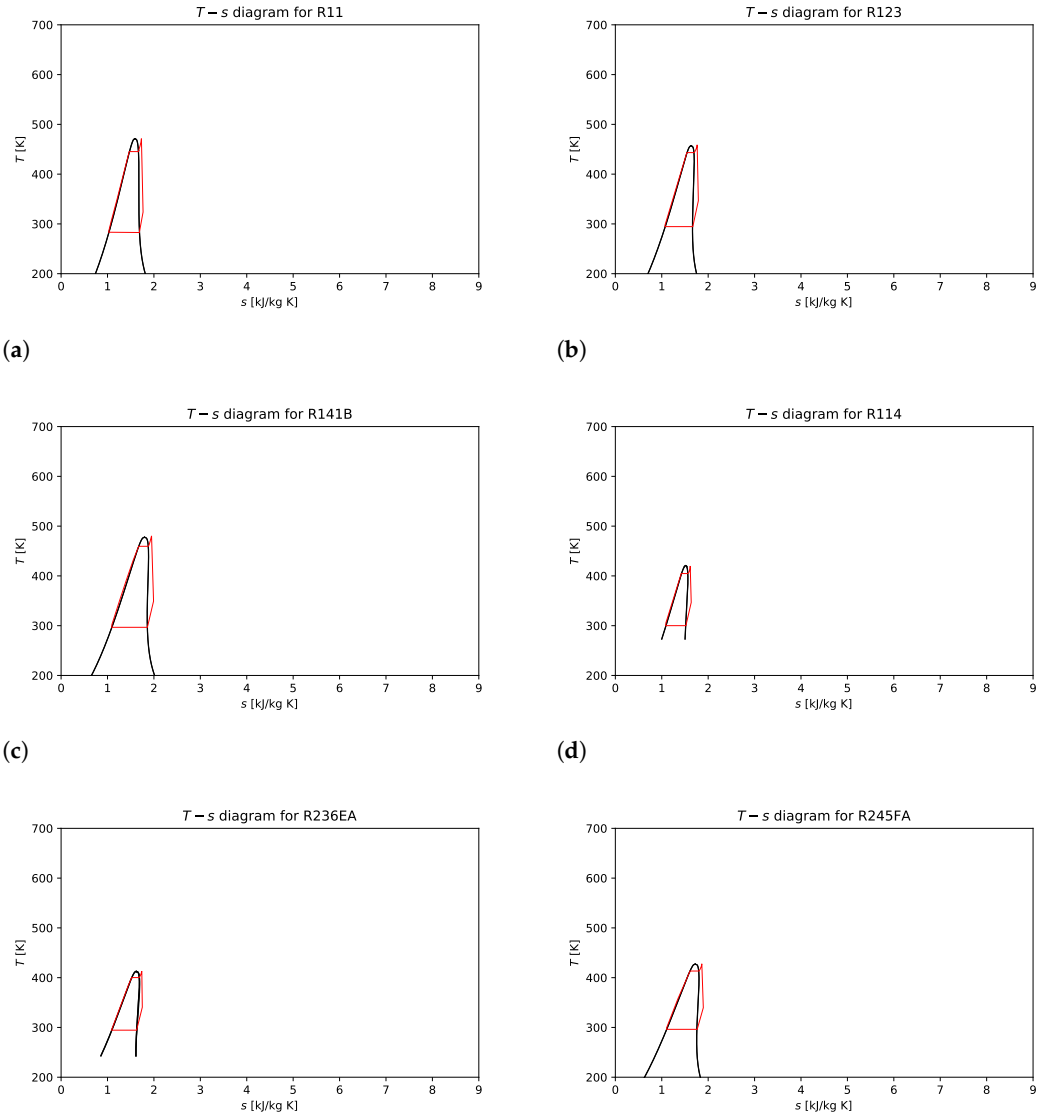

(**a**) (**b**)

(**c**) (**d**)

(**e**) (**f**)

Figure 6. T–s diagrams for fluids of Groups 1 (R11, R123 and R141B) and 2 (R114, R236EA, R245FA). (**a**) R11; (**b**) R123; (**c**) R141B; (**d**) R114; (**e**) R236EA; (**f**) R245FA.

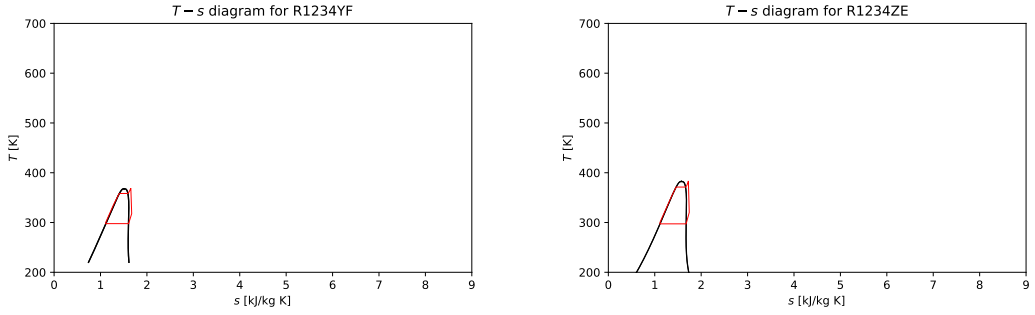

(**a**) (**b**)

Figure 7. *Cont.*

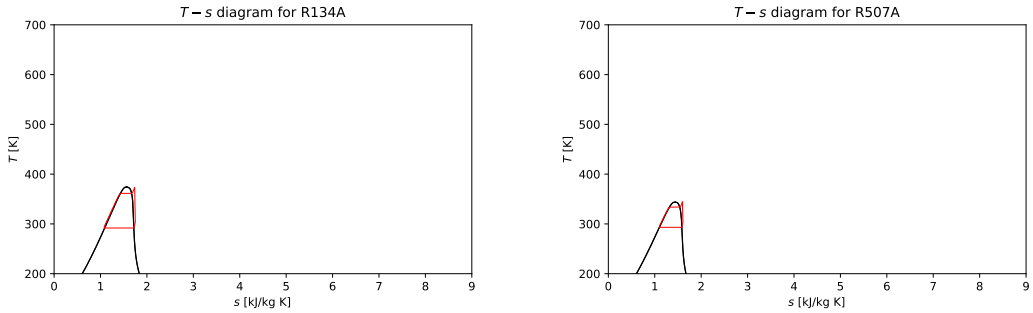

(**c**) (**d**)

Figure 7. T–s diagrams for fluids of Groups 3 (R1234YF, R1234ZE and R134A) and 4 (R507A). (**a**) R1234YF; (**b**) R1234ZE (**c**) R134A; (**d**) R507A.

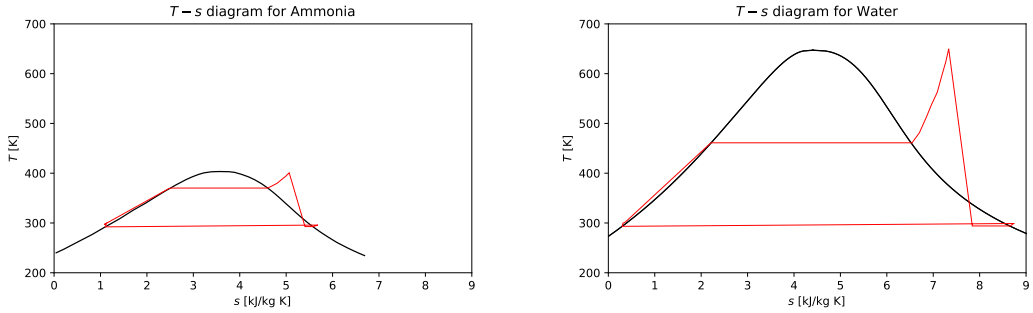

(**a**) (**b**)

Figure 8. T–s diagrams. (**a**) Ammonia; (**b**) water.

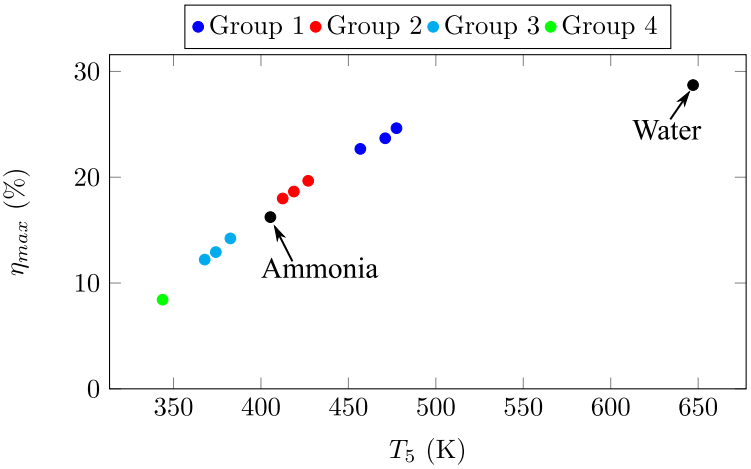

Figure 9. Maximum performance depending on the output super-heater temperature.

The authors have also determined the ORC performance if the inlet turbine temperature is different to the critical value. In such a case, the temperature under analysis is 10 K over the saturated temperature at point 4, see Figure 1. Low GWP and ODP working fluids were analyzed (i.e., R114, R123, R1234YZ and R1234ZE) considering the real cycle. Results are summarized in Table 4. As can be seen, the performance of the ORC is slightly reduced (around 1%) for R114, R1234YF and R1234ZE working fluids; as they present similar temperatures to the critical value. However, the inlet temperature for R123 is reduced by nearly 10%, having a severe impact on the overall performance of the ORC with a reduction of nearly 37%. This fact is in line with the Carnot's cycle performance,

as the higher the temperature difference between cold and hot reservoirs, the higher the equivalent cycle efficiency.

Table 4. Comparison of performance (η) depending on the inlet turbine temperature.

Working Fluid	T_{crit} (K)	$\eta_{T_{crit}}$ (%)	$T_{p_{cald}+10}$ (K)	$\eta_{T_{p_{cald}+10}}$ (%)
R114	418.83	18.65	415.80	18.45
R123	456.83	22.68	419.22	14.33
R1234YZ	367.85	12.22	366.66	12.12
R1234ZE	382.52	14.21	381.14	14.09

5. Conclusions

From the sensibility analysis carried out in this work, varying the super-heater pressure in the ORC shows that the different organic working fluids can be categorized into four main groups. Moreover, in each group except the fourth one, there are low GWP and ODP working fluids, consequently being considered as the optimum fluids to use. Group 1 includes the fluids with lower working pressures (with a pressure in the condenser around 100 kPa) and higher temperatures at the turbine inlet (between 450 and 480 K). These fluids present the higher performance in terms of cycle efficiency (between 23 and 25%) and the optimum fluid to use is R123 due to the low GWP and ODP. As the pressure in the condenser increases, the thermal efficiency of the cycle is progressively reduced, up to values lower than $\eta < 10\%$ for R507A, with a pressure in the condenser around 1100 kPa. Therefore, it is recommended to use fluids with properties similar to the ones described in the fluids of Group 1 to reach higher thermal efficiencies having low GWP and ODP. In the analysis carried out, the maximum super-heating temperature of ORC has been fixed equal to the critical temperature of the fluid used. Therefore, it is possible to obtain a classification of the most suitable fluid depending on the temperature of the heat source available to use. We also conclude that the working fluids with similar turbine inlet temperatures provide similar performances.

Author Contributions: Conceptualization, F.V.-G. and J.A.A.-I.; methodology, A.F.-G.; software, A.F.-G. and F.V.-G.; validation, F.V.-G. and J.A.A.-I.; formal analysis, Á.M.-G.; investigation, A.F.-G. and A.M.-G.; resources, J.A.A.-I.; data curation, F.V.-G.; writing—original draft preparation, A.F.-G. and Á.M.-G.; writing—review and editing, J.A.A.-I.; visualization, Á.M.-G.; supervision, F.V.-G. and J.A.A.-I.; project administration, A.F.-G.; funding acquisition, Á.M.-G. All authors have read and agreed to the published version of the manuscript.

Funding: The author José A. Almendros-Ibáñez would like to acknowledge the financial support of the regional government of Castilla-La Mancha (project SBPLY/17/180501/000412) and the Ministerio de Ciencia, Innovación y Universidades—Agencia Estatal de Investigación (AEI) (RED2018—102431—T).

Institutional Review Board Statement: Not applicable.

Informed Consent Statement: Not applicable.

Conflicts of Interest: The authors declare no conflicts of interest.

Abbreviations

The following abbreviations are used in this manuscript:

ε	Effectiveness
η	Efficiency, performance
cond	Condenser (subscript)
crit	Critical (subscript)
eco	Economizer (subscript)

evap	Evaporator (subscript)
min	Minimum (subscript)
max	Maximum (subscript)
p	Pump (subscript)
reg	Regenerator (subscript)
sh	Super-heater (subscript)
t	Turbine (subscript)
h	Enthalpy
p	Pressure
s	Entropy
v	Volume
x	Quality
Q	Thermal power
T	Temperature
W	Work
GWP	Global warming potential
ICE	Internal combustion engine
ODP	Ozone depleting potential
ORC	Organic Rankine thermodynamic cycle
RC	Rankine thermodynamic cycle
RES	Renewable energy source
WHR	Waste heat recovery

References

1. Jabir, H.J.; Teh, J.; Ishak, D.; Abunima, H. Impacts of Demand-Side Management on Electrical Power Systems: A Review. *Energies* **2018**, *11*, 1050. [CrossRef]
2. Hostick, D.J.; Belzer, D.B.; Hadley, S.W.; Markel, T.; Marnay, C.; Kintner-Meyer, M.C. *Projecting Electricity Demand in 2050*; Technical Report; Pacific Northwest National Lab. (PNNL): , Richland, WA, USA, 2014.
3. Ram, M.; Bogdanov, D.; Aghahosseini, A.; Oyewo, S.; Gulagi, A.; Child, M.; Fell, H.J.; Breyer, C. *Global Energy System Based on 100% Renewable Energy—Power Sector*; Lappeenranta University of Technology and Energy Watch Group: Lappeenranta, Finland, 2017.
4. International Renewable Energy Agency (IRENA). *Renewable Energy Prospects for the European Union*; International Renewable Energy Agency (IRENA): Abu Dhabi, United Arab Emirates; European Commission (EC): Brussels, Belgium, 2018.
5. Fernández-Guillamón, A.; Das, K.; Cutululis, N.A.; Molina-García, Á. Offshore wind power integration into future power systems: Overview and trends. *J. Mar. Sci. Eng.* **2019**, *7*, 399. [CrossRef]
6. Koirala, B.P.; Koliou, E.; Friege, J.; Hakvoort, R.A.; Herder, P.M. Energetic communities for community energy: A review of key issues and trends shaping integrated community energy systems. *Renew. Sustain. Energy Rev.* **2016**, *56*, 722–744. [CrossRef]
7. UNFCCC. INDC—Submissions n.d. Technical Report. Intended Nationally Determined Contributions. 2020. Available online: http://www4.unfccc.int (accessed on 2 March 2021).
8. Decc, D. *Community Energy Strategy: Full Report*; Department of Energy and Climate Change: London, UK, 2014.
9. European Commission. *2030 Climate & Energy Framework*. Technical Report; European Commission: Brussels, Belgium, 2020. Available online: https://ec.europa.eu/clima/policies/strategies/2030_en (accessed on 2 March 2021).
10. *Data and Statistics*. International Energy Agency. Available online: https://www.iea.org/data-and-statistics (accessed on 2 March 2021).
11. Saleh, B.; Koglbauer, G.; Wendland, M.; Fischer, J. Working fluids for low-temperature organic Rankine cycles. *Energy* **2007**, *32*, 1210–1221. [CrossRef]
12. Tchanche, B.F.; Pétrissans, M.; Papadakis, G. Heat resources and organic Rankine cycle machines. *Renew. Sustain. Energy Rev.* **2014**, *39*, 1185–1199. [CrossRef]
13. Lemmens, S. Cost engineering techniques and their applicability for cost estimation of organic Rankine cycle systems. *Energies* **2016**, *9*, 485. [CrossRef]
14. Wang, L.; Yang, Z.; Sharma, S.; Mian, A.; Lin, T.E.; Tsatsaronis, G.; Maréchal, F.; Yang, Y. A Review of Evaluation, Optimization and Synthesis of Energy Systems: Methodology and Application to Thermal Power Plants. *Energies* **2019**, *12*, 73. [CrossRef]
15. Desideri, A.; Gusev, S.; van den Broek, M.; Lemort, V.; Quoilin, S. Experimental comparison of organic fluids for low temperature ORC (organic Rankine cycle) systems for waste heat recovery applications. *Energy* **2016**, *97*, 460–469. [CrossRef]
16. Zhao, Y.; Liu, G.; Li, L.; Yang, Q.; Tang, B.; Liu, Y. Expansion devices for organic Rankine cycle (ORC) using in low temperature heat recovery: A review. *Energy Convers. Manag.* **2019**, *199*, 111944. [CrossRef]
17. Yu, H.; Gundersen, T.; Feng, X. Process integration of organic Rankine cycle (ORC) and heat pump for low temperature waste heat recovery. *Energy* **2018**, *160*, 330–340. [CrossRef]
18. Hossain, S.N.; Bari, S. Waste heat recovery form the exahust of diesel generator using Rankine Cycle. *Energy Convers. Manag.* **2013**, *75*, 141–151. [CrossRef]

19. Saidur, R.; Rezaei, M.; Muzammil, W.; Hassan, M.; Paria, S.; Hasanuzzaman, M. Technologies to recover exhaust heat from internal combustion engines. *Renew. Sustain. Energy Rev.* **2012**, *16*, 5649–5659. [CrossRef]
20. Sahlot, M.; Riffat, S.B. Desiccant cooling systems: A review. *Int. J. Low-Carbon Technol.* **2016**, *11*, 489–505. [CrossRef]
21. European Parliament and the Council of the European Union. Directive 2006/40/EC of The European Parliament and of the Council of 17 May 2006 relating to emissions from air conditioning systems in motor vehicles and amending Council Directive 70/156/EC. *Off. J. Eur. Union L* **2006**. *161*, 1–11.
22. European Parliament and the Council of the European Union. Regulation (EU) No 517/2014 of the European Parliament and the Council of 16 April 2014 on fluorinated greenhouse gases and repealing Regulation (EC) No 842/2006. *Off. J. Eur. Union L* **2014**. *150*, 195–230.
23. Calm, J.M. The next generation of refrigerants—Historical review, considerations, and outlook. *Int. J. Refrig.* **2008**, *31*, 1123–1133. [CrossRef]
24. Pérez-García, V.; Belman-Flores, J.M.; Rodríguez-Muñoz, J.L.; Rangel-Hernández, V.; Gallegos-Muñoz, A. Second law analysis of a mobile air conditioning system with internal heat exchanger using low GWP refrigerants. *Entropy* **2017**, *19*, 175. [CrossRef]
25. Portmann, R.; Daniel, J.; Ravishankara, A. Stratospheric ozone depletion due to nitrous oxide: Influences of other gases. *Philos. Trans. R. Soc. B Biol. Sci.* **2012**, *367*, 1256–1264. [CrossRef]
26. Mota-Babiloni, A.; Navarro-Esbrí, J.; Makhnatch, P.; Molés, F. Refrigerant R32 as lower GWP working fluid in residential air conditioning systems in Europe and the USA. *Renew. Sustain. Energy Rev.* **2017**, *80*, 1031–1042. [CrossRef]
27. Jiang, L.; Lu, H.; Wang, L.; Gao, P.; Zhu, F.; Wang, R.; Roskilly, A. Investigation on a small-scale pumpless Organic Rankine Cycle (ORC) system driven by the low temperature heat source. *Appl. Energy* **2017**, *195*, 478–486. [CrossRef]
28. Yang, J.; Ye, Z.; Yu, B.; Ouyang, H.; Chen, J. Simultaneous experimental comparison of low-GWP refrigerants as drop-in replacements to R245fa for Organic Rankine cycle application: R1234ze (Z), R1233zd (E), and R1336mzz (E). *Energy* **2019**, *173*, 721–731. [CrossRef]
29. Gil, B.; Kasperski, J. Efficiency evaluation of the ejector cooling cycle using a new generation of HFO/HCFO refrigerant as a R134a replacement. *Energies* **2018**, *11*, 2136. [CrossRef]
30. Saengsikhiao, P.; Taweekun, J.; Maliwan, K.; Sae-ung, S.; Theppaya, T. Investigation and Analysis of R463A as an Alternative Refrigerant to R404A with Lower Global Warming Potential. *Energies* **2020**, *13*, 1514. [CrossRef]
31. Ayachi, F.; Ksayer, E.B.; Zoughaib, A.; Neveu, P. ORC optimization for medium grade heat recovery. *Energy* **2014**, *68*, 47–56. [CrossRef]
32. Feng, Y.Q.; Luo, Q.H.; Wang, Q.; Wang, S.; He, Z.X.; Zhang, W.; Wang, X.; An, Q.S. Entropy and Entransy Dissipation Analysis of a Basic Organic Rankine Cycles (ORCs) to Recover Low-Grade Waste Heat Using Mixture Working Fluids. *Entropy* **2018**, *20*, 818. [CrossRef] [PubMed]
33. Rak, J.; Błasiak, P.; Kolasiński, P. Influence of the applied working fluid and the arrangement of the steering edges on multi-vane expander performance in micro ORC system. *Energies* **2018**, *11*, 892.
34. Meinel, D.; Wieland, C.; Spliethoff, H. Effect and comparison of different working fluids on a two-stage organic rankine cycle (ORC) concept. *Appl. Therm. Eng.* **2014**, *63*, 246–253. [CrossRef]
35. Matuszewska, D.; Olczak, P. Evaluation of using gas turbine to increase efficiency of the Organic Rankine Cycle (ORC). *Energies* **2020**, *13*, 1499. [CrossRef]
36. Zeleny, Z.; Vodicka, V.; Novotny, V.; Mascuch, J. Gear pump for low power output ORC–an efficiency analysis. *Energy Procedia* **2017**, *129*, 1002–1009. [CrossRef]
37. Pan, M.; Lu, F.; Zhu, Y.; Huang, G.; Yin, J.; Huang, F.; Chen, G.; Chen, Z. Thermodynamic, exergoeconomic and multi-objective optimization analysis of new ORC and heat pump system for waste heat recovery in waste-to-energy combined heat and power plant. *Energy Convers. Manag.* **2020**, *222*, 113200. [CrossRef]
38. Delgado-Torres, A.M.; García-Rodríguez, L. Preliminary design of seawater and brackish water reverse osmosis desalination systems driven by low-temperature solar organic Rankine cycles (ORC). *Energy Convers. Manag.* **2010**, *51*, 2913–2920. [CrossRef]
39. Ge, Z.; Wang, H.; Wang, H.T.; Wang, J.J.; Li, M.; Wu, F.Z.; Zhang, S.Y. Main parameters optimization of regenerative organic Rankine cycle driven by low-temperature flue gas waste heat. *Energy* **2015**, *93*, 1886–1895. [CrossRef]
40. Li, M.; Wang, J.; He, W.; Gao, L.; Wang, B.; Ma, S.; Dai, Y. Construction and preliminary test of a low-temperature regenerative Organic Rankine Cycle (ORC) using R123. *Renew. Energy* **2013**, *57*, 216–222. [CrossRef]
41. Petrollese, M.; Oyekale, J.; Tola, V.; Cocco, D. Optimal ORC configuration for the combined production of heat and power utilizing solar energy and biomass. In Proceedings of the ECOS, Guimarães, Portugal, 17–21 June 2018; pp. 17–22.
42. Moran, M.J.; Shapiro, H.N.; Boettner, D.D.; Bailey, M.B. *Fundamentals of Engineering Thermodynamics*; John Wiley & Sons: Hoboken, NJ, USA, 2010.
43. Khennich, M.; Galanis, N. Optimal design of ORC systems with a low-temperature heat source. *Entropy* **2012**, *14*, 370–389. [CrossRef]
44. Györke, G.; Groniewsky, A.; Imre, A.R. A simple method of finding new dry and isentropic working fluids for organic rankine cycle. *Energies* **2019**, *12*, 480. [CrossRef]
45. López-Belchí, A.; Illán-Gómez, F.; Vera-García, F.; García-Cascales, J.R. Experimental condensing two-phase frictional pressure drop inside mini-channels. Comparisons and new model development. *Int. J. Heat Mass Transf.* **2014**, *75*, 581–591. [CrossRef]

46. López-Belchí, A.; Illan-Gomez, F.; Cano-Izquierdo, J.M.; García-Cascales, J.R. GMDH ANN to optimise model development: Prediction of the pressure drop and the heat transfer coefficient during condensation within mini-channels. *Appl. Therm. Eng.* **2018**, *144*, 321–330. [CrossRef]
47. Bell, I.H.; Wronski, J.; Quoilin, S.; Lemort, V. Pure and Pseudo–pure Fluid Thermophysical Property Evaluation and the Open-Source Thermophysical Property Library CoolProp. *Ind. Eng. Chem. Res.* **2014**, *53*, 2498–2508. [CrossRef] [PubMed]
48. Quoilin, S.; Declaye, S.; Tchanche, B.F.; Lemort, V. Thermo-economic optimization of waste heat recovery Organic Rankine Cycles. *Appl. Therm. Eng.* **2011**, *31*, 2885–2893. [CrossRef]
49. Benhadid-Dib, S.; Benzaoui, A. Refrigerants and their environmental impact Substitution of hydro chlorofluorocarbon HCFC and HFC hydro fluorocarbon. Search for an adequate refrigerant. *Energy Procedia* **2012**, *18*, 807–816. [CrossRef]
50. Mota-Babiloni, A.; Navarro-Esbrí, J.; Barragán, Á.; Molés, F.; Peris, B. Drop-in energy performance evaluation of R1234yf and R1234ze (E) in a vapor compression system as R134a replacements. *Appl. Therm. Eng.* **2014**, *71*, 259–265. [CrossRef]
51. Abas, N.; Nawaz, R.; Khan, N. Parametric quantification of low GWP refrigerant for thermosyphon driven solar water heating system. *Procedia Comput. Sci.* **2015**, *52*, 804–811. [CrossRef]
52. Fannou, J.L.C.; Rousseau, C.; Lamarche, L.; Kajl, S. A comparative performance study of a direct expansion geothermal evaporator using R410A and R407C as refrigerant alternatives to R22. *Appl. Therm. Eng.* **2015**, *82*, 306–317. [CrossRef]
53. Petrovic, A.; Delibasic, B.; Filipovic, J.; Petrovic, A.; Lomovic, M. Thermoeconomic and environmental optimization of geothermal water desalination plant with ejector refrigeration system. *Energy Convers. Manag.* **2018**, *178*, 65–77. [CrossRef]
54. López-Belchí, A. Assessment of a mini-channel condenser at high ambient temperatures based on experimental measurements working with R134a, R513A and R1234yf. *Appl. Therm. Eng.* **2019**, *155*, 341–353. [CrossRef]
55. Janković, Z.; Atienza, J.S.; Suárez, J.A.M. Thermodynamic and heat transfer analyses for R1234yf and R1234ze (E) as drop-in replacements for R134a in a small power refrigerating system. *Appl. Therm. Eng.* **2015**, *80*, 42–54. [CrossRef]
56. Yataganbaba, A.; Kilicarslan, A.; Kurtbaş, İ. Exergy analysis of R1234yf and R1234ze as R134a replacements in a two evaporator vapour compression refrigeration system. *Int. J. Refrig.* **2015**, *60*, 26–37. [CrossRef]
57. Sánchez, D.; Cabello, R.; Llopis, R.; Arauzo, I.; Catalán-Gil, J.; Torrella, E. Energy performance evaluation of R1234yf, R1234ze (E), R600a, R290 and R152a as low-GWP R134a alternatives. *Int. J. Refrig.* **2017**, *74*, 269–282. [CrossRef]